Journal of Anatomy

J. Anat. (2011) **219**, pp676–695 doi: 10.1111/j.1469-7580.2011.01437.x

The head of the finch: the anatomy of the feeding system in two species of finches (*Geospiza fortis* and *Padda oryzivora*)

Annelies Genbrugge,[1,2] Anthony Herrel,[3,4] Matthieu Boone,[5] Luc Van Hoorebeke,[5] Jeffrey Podos,[6] Joris Dirckx,[1] Peter Aerts[4,7] and Adriaens Dominique[2]

[1]*Laboratory of Biomedical Physics, University of Antwerp, Antwerpen, Belgium*
[2]*Evolutionary Morphology of Vertebrates, Ghent University, Gent, Belgium*
[3]*Département d'Ecologie et de Gestion de la Biodiversité, Museum National d'Histoire Naturelle, Paris, France*
[4]*Department of Biology, University of Antwerp, Antwerpen, Belgium*
[5]*UGCT, Department of Physics and Astronomy, Ghent University, Institute for Nuclear Sciences (INW), Gent, Belgium*
[6]*Department of Biology and Graduate Program in Organismic and Evolutionary Biology, University of Massachusetts, Amherst, MA, USA*
[7]*Department of Movement and Sports Sciences, Ghent University, Gent, Belgium*

Abstract

Despite the large number of studies devoted to the evolution of beak shape in Darwin's finches, surprisingly little is known about the morphology of the skull and jaw musculature in these birds. Moreover, it remains currently unclear whether Darwin's finches are unusual in their cranial morphology compared with other seed-cracking birds. Here, we provide a detailed description of the morphology of the cranial system in the medium ground finch (*Geospiza fortis*) and compare it with that of another seed-cracking bird of similar overall size and appearance, the Java finch (*Padda oryzivora*). Our data show an overall similarity in beak size and cranial morphology. Yet, differences in the jaw adductor size and corresponding attachments to the cranium and mandible are prominent, with the medium ground finch having much more robust jaw-closing muscles. This is reflected in differences in bite forces, with the medium ground finch biting much harder than the Java finch. These data suggest similarities in the evolution of the feeding system in birds specializing in the cracking of hard seeds, but also show the uniqueness of the cranial morphology and bite force of the medium ground finch compared with other seed-cracking birds.

Key words: Darwin's finches; jaw musculature; skull morphology.

Introduction

Ever since Darwin first drew attention to the finches of the Galápagos and Cocos Islands, and their variation in beak shape (Darwin, 1841), these birds have become a model system in evolutionary biology. The remarkable variation in beak size and shape associated with a specialization of these birds on different food resources coupled with the rapid divergence from a common ancestor make this group of birds a textbook example of an adaptive radiation (Grant, 1986; Schluter, 2000). The prominent differences in beak morphology, ranging from long pointed beaks in the warbler finch (*Certhidea olivacea*) to the deep and wide beaks as observed in the ground finches of the genus *Geospiza*, have been shown to be related to differences in the size and hardness of the selected food items (Bowman, 1961; Grant, 1986). Moreover, habitat structure and food availability determine the species composition on the different islands of the Galápagos (Grant, 1986).

Previous studies on Darwin's finches have mainly focused on how variation in beak shape is related to variation in food preference (Bowman, 1961; Boag & Grant, 1981; Schluter, 1982; Grant, 1986; Grant & Grant, 2008), and the underlying genetic basis and control of beak development (Abzhanov et al. 2004, 2006). Despite the wealth of studies focusing on variation in external beak morphology (Schluter, 1984; Grant, 1986; Grant & Grant, 2002; Podos & Nowicki, 2004; Kleindorfer et al. 2006; Foster et al. 2008), only a single study has examined the musculoskeletal structure of the feeding apparatus in Darwin's finches (Bowman, 1961). The study by

Correspondence
Annelies Genbrugge, Evolutionary Morphology of Vertebrates, Ghent University, K.L. Ledeganckstraat 35, 9000 Gent, Belgium.
T: ++32 9 264 52 20; F: ++32 9 264 53 44;
E: annelies.genbrugge@ugent.be

Accepted for publication *9 September 2011*
Article published online *17 October 2011*

Bowman (1961) focused on the variation in muscle mass, muscle origin and the shape of the skull in Darwin's finches in relation to differences in diet. However, already in 1963, Bock pointed out some shortcomings in the paper published by Bowman (1961), including the lack of a description of the ligaments, the angle of insertion of the muscles, the length of the lever arms and the degree of pennation of the muscles. In addition, a detailed morphological description of the osteology, arthrology and myology of the head of Darwin's finches is currently still lacking, despite its relevance for a thorough understanding of the evolutionary transformations in the cranial system that lie at the base of the adaptive radiation in these emblematic animals.

A better understanding of the detailed anatomy of the feeding apparatus is indeed crucial in assessing the adaptive nature of the observed phenotypic variation. Unfortunately, the protected status of the Darwin's finches and the inability to obtain fresh specimens precludes functional analysis in relation to seed-crushing performance, which is needed to link morphology to function and ecology and to validate the output of finite element models that have recently been developed (Herrel et al. 2010; Soons et al. 2010). Finding a suitable model species that could serve as a proxy for Darwin's finches, but that can be easily obtained and bred in captivity, could partially overcome this problem. Here, we explore whether the Java finch (*Padda oryzivora*), a distantly related seed-cracking passeriform (Jønsson & Fjeldså, 2006), can be considered a suitable model for one type of Darwin's finch (i.e. the hard seed crushers) by comparing the anatomy of its feeding apparatus. In particular this species was chosen as it is a specialized seed crusher and has, apart from its color, a similar external appearance compared with the medium ground finch (*Geospiza fortis*; Fig. 1). Indeed, Colnett (1798) already compared the Darwin's finches with the Java finches in his book about his voyage to the South Atlantic (and the Galápagos): 'There were also small birds, … resembling the Java sparrow, in shape and size, but of a black plumage; ...'

The principal aim of our study thus is to provide a detailed description of the osteology, arthrology and myology of the jaw apparatus in the medium ground finch, *G. fortis*. Secondly, we compare the anatomy of the cranial system in the medium ground finch with that of the Java finch (*P. oryzivora*) to explore its suitability as an appropriate functional analog that could be used for future functional and experimental analyses.

Materials and methods

Specimens

The analyzed material comprises four adult specimens of the medium ground finch (*G. fortis*) and six adult specimens of the Java finch (*P. oryzivora*). Road-killed ground finches were collected during February–March of 2005 and 2006 on Santa Cruz Island under a salvage permit from the Galápagos National Park Service. Intact specimens were preserved in a 10% aqueous formaldehyde solution for 24 h, rinsed and transferred to a 70% aqueous ethanol solution. The *P. oryzivora* were captive-bred animals obtained from commercial suppliers in Belgium and killed by a veterinarian of the Faculty of Veterinary Medicine at Ghent University. The specimens were preserved in a 10% aqueous formaldehyde solution for 4 weeks, rinsed and transferred to a 70% aqueous ethanol solution.

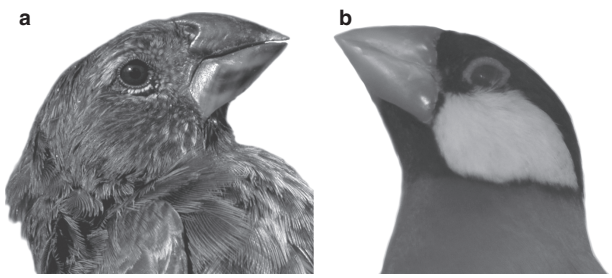

Fig. 1 Comparison of the external morphology of *Geospiza fortis* (a) and *Padda oryzivora* (b). Illustrated is a lateral view of the head of both species; note the similarity in beak size and shape.

The *P. oryzivora* and *G. fortis* specimens were measured (head length, head width, head depth, beak length, beak width, beak depth, tarsus length and wing chord) with a digital calliper (Mauser digital, accuracy of 0.01 mm) following Grant (1986) and Herrel et al. (2005a). In Table 1, head dimensions, tarsus length and the wing chord are shown for both species.

CT-scanning and 3D-reconstruction

All specimens were scanned at the UGCT scanning facility at Ghent University (http://www.ugct.ugent.be) using a micro-focus transmission-type X-ray tube. Depending on sample size, tube voltage was chosen between 80 and 100 kV, and an open type dual head tube (Feinfocus FXE160.50 and FXE160.51) was used providing sufficiently small spot size. Specimens were mounted on a controllable rotating table (MICOS, UPR160F-AIR). For each specimen a series of 1000 projections of 1496 × 1880 pixels was recorded, covering 360 °. Reconstruction of the tomographic projection data was done using the in-house developed Octopus-package (Vlassenbroeck et al. 2007). Volume and surface rendering was performed using Amira 5.2.0 (64-bit version, Computer Systems Mercury).

Table 1 Table summarizing differences in head and body dimensions between the two species studied in this study.

	Geospiza fortis (n = 4)	*Padda oryzivora* (n = 6)
Beak length (mm)	13.67 ± 3.84	14.13 ± 2.25
Beak depth (mm)	12.68 ± 1.34	12.17 ± 0.41
Beak width (mm)	9.82 ± 1.18	9.95 ± 0.92
Head length (mm)	33.51 ± 1.71	31.90 ± 0.68
Head depth (mm)	17.65 ± 0.91	15.98 ± 1.11
Head width (mm)	17.75 ± 0.81	15.94 ± 1.19
Tarsus length (mm)	23.95 ± 2.00	21.06 ± 1.00
Wing chord (mm)	73.19 ± 5.90	69.40 ± 1.33

Table entries are means ± standard deviations.

Bite forces

Bite force data of the five *P. oryzivora* were measured using a Kistler piezoelectric force transducer (type 9203, Kistler, Switzerland; ± 500 N) mounted in a custom-built holder, and connected to a portable Kistler charge amplifier (type 5059A). A detailed description of this setup is available in Herrel et al. (2005a,b). The bite force data for *G. fortis* were taken from Herrel et al. (2005a).

Muscle properties

The description of the arthrology and myology are based on dissections of five *P. oryzivora* and four *G. fortis*. Dissections were done using a binocular microscope (Olympus SZX7). For four *P. oryzivora* and four *G. fortis*, all jaw muscle bundles were removed individually during the dissections. Muscles were blotted dry and weighted on an OHAUS Adventurer microbalance (± 0.1 mg) following Soons et al. (2010). Muscles were transferred to a 30% aqueous nitric acid solution for 24 h to digest the connective tissue and transferred to a 50% aqueous glycerol solution (Loeb & Gans, 1986). Fibers were teased apart using blunt-tipped glass needles and drawn using a dissecting scope with camera lucida. Alternatively, pictures were taken with a Nikon d40 × digital camera with macro lens. Next, drawings of the *G. fortis* specimens fibers were scanned and fiber lengths were determined using NIH image. For the four *P. oryzivora* specimens, fiber lengths were measured using the software program AnalySIS 5.0 (Soft Imaging System gmbH, Germany). Muscle physiological cross-sectional area (PCSA) of each muscle bundle was calculated by dividing muscle mass (g), multiplied by muscle density (1.065 g cm^{-3}; Méndez & Keys, 1960), by fiber length (cm). The muscle mass, muscle fiber length and PCSA of each muscle bundle are listed in Table 2.

Although the quantification of muscle architecture may have errors associated (e.g. weighing errors, fiber shrinkage after death; Cutts, 1988), our results give a reasonable approximation of the differences in cross-sectional area between species. We did not correct PCSA values for pennation angles as pennation angles are known to vary during contraction (Muhl, 1982; Litchwark et al. 2007; Azizi et al. 2008).

Statistical analyses

All morphometric data were Log_{10}-transformed before analysis to meet assumptions of normality and homoscedascity for parametric statistics. First we tested whether species were different in two measures typically used as indicators of body size: tarsus length and wing chord. As differences between species were not significant (MANOVA: Wilk's lambda = 0.55; $F_{2,3} = 1.24$; $P = 0.41$), subsequent analyses were performed on uncorrected data. Next we tested whether species differed in beak size, head size, bite force, muscle mass, muscle fiber lengths and PCSA using MANOVAs. All statistical analyses were performed using the software program SPSS V.15 (Statsoft).

Results

The following descriptions start with a detailed description of *G. fortis*, followed by a short enumeration of the differences observed in *P. oryzivora*. The anatomical nomenclature used is based on the Nomina Anatomica Avium (Baumel et al. 1979). Some additional terms are used, and are based on Nuijens & Zweers (1997).

Osteology and arthrology

Statistical results

A MANOVA, testing for differences in beak dimensions between species, detected no differences (Wilks' lambda = 0.17; $F_{3,2} = 3.23$; $P = 0.25$). Differences in head dimensions approached significance (Wilks' lambda = 0.035; $F_{3,2} = 18.35$; $P = 0.052$). Univariate ANOVAs demonstrated that differences were significant in head width ($F_{1,4} = 38.27$; $P = 0.003$) and depth ($F_{1,4} = 23.87$; $P = 0.008$), but not head length ($F_{1,4} = 4.43$; $P = 0.10$).

Braincase

Only those parts that are associated to the attachment of the jaw muscles will be described here: the lateral side of the cranium, the septum interorbitale and the caudal wall of the orbits.

Geospiza fortis (Figs 2–4). The lateral side of the cranium is characterized by a large fossa and three processes. The processus postorbitalis forms the dorsocaudal edge of the orbit and extends ventrally. It has a crista (Cr1) on its medioventral side, which runs mediocaudally and turns in a ventrolateral direction, and a crista (Cr2) on its laterocaudal edge, running dorsocaudally. The latter crista forms the rostral border of the large lateral fossa temporalis. Dorsally and caudally this fossa is bordered by the crista temporalis and ventrally by another crista (Cr3). The crista temporalis and the latter crista come together in a rostroventrally pointing spine (Sp1). In the center of the fossa temporalis emerges a second process, the processus zygomaticus. This is a very large, dorsoventrally flattened, rostroventrally pointing process that carries three cristae: one laterally (Cr4), one ventrally (Cr5) and one rostromedially (Cr6). The third process, the processus suprameaticus, lies on the lateral side of the braincase, is smaller and points ventrally. Caudoventrally to the processus suprameaticus lies the processus paroccipitalis as a wing-like, rostrally oriented process partially covering the cavum tympanicum. The caudal end of the latter process is marked by the lateral part of the arched crista nuchalis transversa, running further along the caudal side of the cranium. The ventrolateral side of the braincase is characterized by two round articular sockets, rostromedial to the processus paroccipitalis, which articulate with the two articular heads of the processus oticus of the os quadratum. The lateral-most socket lies at the ventrolateral tip of the processus suprameaticus and articulates with the condylus squamosum of the processus oticus quadrati, while the other, which lies somewhat mediocaudal to the first, articulates with the condylus prooticus of the same process.

Table 2 Summary of the muscle mass, fiber length and PCSA of each muscle bundle of the two species of finches included in our study.

	M. depressor mandibulae	M. adductor mandibulae externus rostralis	M. adductor mandibulae externus ventralis	M. adductor mandibulae externus profundus	M. adductor mandibulae ossis quadrati	M. pseudotemporalis superficialis lateralis	M. pseudotemporalis superficialis medialis	M. pseudotemporalis profundus	M. pterygoideus ventralis lateralis	M. pterygoideus ventralis medialis	M. pterygoideus dorsalis lateralis	M. pterygoideus dorsalis medialis	M. retractor palatini	M. protractor pterygoidei et quadrati
Fiber length (mm)														
Geospiza	3.91	1.99	1.60	1.83	2.02	1.31	2.06	3.58	2.38	2.52	2.07	1.73	2.88	3.40
fortis (*n* = 4)	± 0.41	± 0.59	± 0.27	± 0.43	± 0.26	± 0.25	± 0.69	± 0.16	± 0.15	± 0.06	± 0.30	± 0.70	± 0.45	± 0.42
Padda	3.28	1.46	1.27	1.34	1.64	1.36	1.49	2.55	2.02	2.13	2.02	1.67	2.21	2.06
oryzivora (*n* = 4)	± 0.28	± 0.08	± 0.14	± 0.13	± 0.31	± 0.48	± 0.49	± 0.49	± 0.12	± 0.11	± 0.29	± 0.26	± 0.38	± 0.08
Muscle mass (mg)														
G. fortis	23.18	65.13	15.93	21.65	2.60	9.38	12.4	28.3	19.9	11.85	28.35	33.33	4.13	5.9
(*n* = 4)	± 6.14	± 22.17	± 5.64	± 5.05	± 0.57	± 8.33	± 3.62	± 6.28	± 7.54	± 2.56	± 6.94	± 16.05	± 0.63	± 1.93
P. oryzivora	11.5	23.38	3.87	8.88	2.88	3.38	4.38	7.13	10.17	4.67	17.83	7.5	6.38	3.75
(*n* = 4)	± 2.38	± 3.40	± 1.03	± 1.93	± 1.44	± 1.89	± 1.60	± 1.32	± 2.57	± 2.08	± 2.75	± 1.80	± 1.60	± 0.96
PCSA (mm^2)														
G. fortis	5.02	29.38	8.26	10.63	1.14	3.75	5.71	7.40	7.86	4.06	13.83	16.43	1.37	1.11
(*n* = 4)	± 1.24	± 14.04	± 2.97	± 4.14	± 0.33	± 2.25	± 2.01	± 2.33	± 3.87	± 0.74	± 5.81	± 9.78	± 0.22	± 0.40
P. oryzivora (*n* = 4)	3.28	15.10	2.85	6.18	1.63	2.26	3.06	2.67	4.76	2.07	8.33	4.24	2.79	1.70
	± 0.54	± 2.35	± 0.70	± 1.06	± 0.77	± 0.97	± 1.64	± 0.56	± 1.14	± 1.00	± 0.99	± 1.03	± 0.91	± 0.40

Table entries are means ± standard deviations.
PCSA, physiological cross-sectional area.

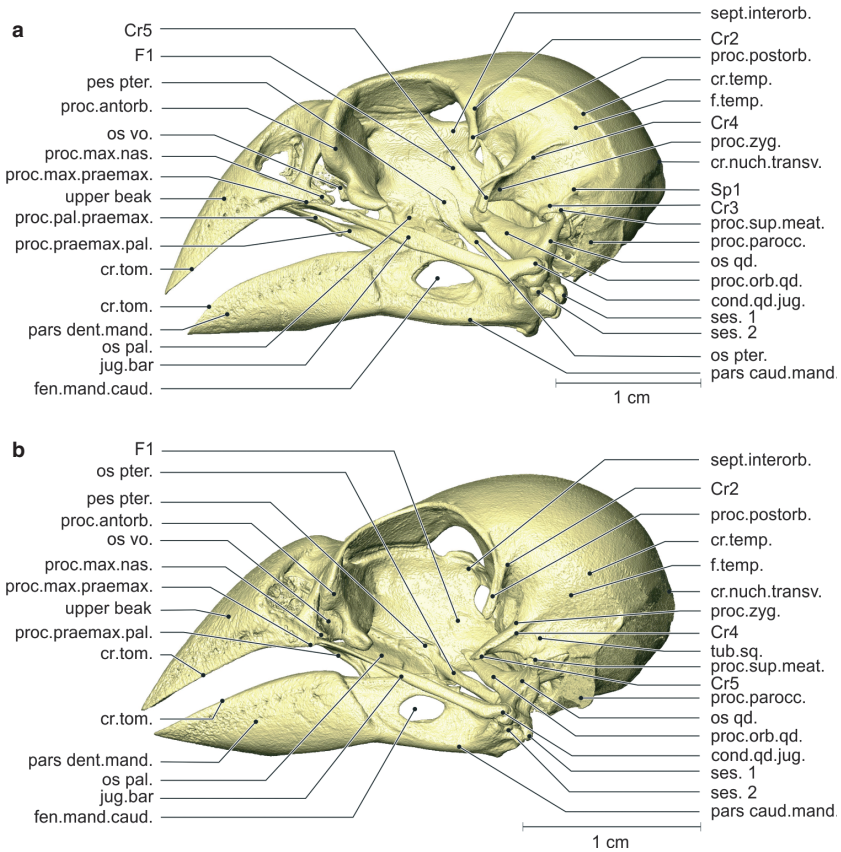

Fig. 2 Osteology. Lateral view of the left side of the skull of *Geospiza fortis* (a) and *Padda oryzivora* (b). Note that the crista temporalis and the processus antorbitalis are much more prominent in *G. fortis*. The beaks, however, have more or less the same shape. cond.qd.jug., condylus quadrati jugalis; cr.nuch.transv., crista nuchalis transversa; cr.temp., crista temporalis; cr.tom., crista tomialis; fen.mand.caud., fenestra mandibulae caudalis; f.temp., fossa temporalis; os pal., os palatinum; os pter., os pterygoideum; os qd., os quadratum; os vo., os vomer; pars caud.mand., pars caudalis mandibulae; pars dent.mand., pars dentalis mandibulae; pes pter., pes pterygoidei; proc.antorb., processus antorbitalis; proc.max.praemax., processus maxillaris praemaxillae; proc.orb.qd., processus orbitalis quadrati; proc.pal.praemax., processus palatinus praemaxillae; proc.parocc., processus paroccipitalis; proc.postorb., processus postorbitalis; proc.praemax.pal., processus praemaxillaris palatini; proc.sup.meat., processus suprameaticus; proc.zyg., processus zygomaticus; sept.interorb., septum interorbitalis; ses. 1, first sesamoid bone; ses. 2, second sesamoid bone; tub.sq., tuberculum squamosum.

The caudal wall of the orbit forms the large fossa parietalis caudalis orbitalis, which is divided by two prominent rostrocaudal cristae (Cr7 and Cr8) and dorsally bordered by a smaller crista (Cr1′). The lateral edge of this fossa is formed by the medioventral crista of the processus postorbitalis (Cr1). The rostral wall of the orbit is formed by a robust processus antorbitalis. Caudally, the interorbital septum bears a small and shallow fossa (F1) that is ventrocaudally oriented. The medioventral side of the braincase is characterized by a thin, triangular plate, the basis rostri parasphenoidalis, which projects rostrally and partially covering the caudal part of the rostrum parasphenoidale. Rostral to this plate, two small cristae (Cr9) can be found, starting caudolaterally and running mediorostrally to meet at the caudal base of the rostrum parasphenoidale.

Padda oryzivora (Figs 2–4). Some minor differences can be observed on the lateral side of the braincase. The processus postorbitalis is situated more ventrally and is longer. The processus zygomaticus has more or less the same shape, but is not as strongly developed. Moreover, the crista temporalis, Cr3 and the crista nuchalis transversa are less prominent. The processus paroccipitalis is smaller and does not extend as far dorsally. Between the processus zygomaticus and the processus suprameaticus a small tubercle can be found, the tuberculum squamosum. The fossa parietalis caudalis orbitalis is much smaller and situated more ventrally. Also, the associated cristae (Cr7, Cr8 and Cr1′) are less developed. The processus antorbitalis is clearly less prominent. On the ventral side of the braincase, the two cristae (Cr9) are, however, larger, and the rostrum parasphenoidale is much narrower. The lateral-most socket on the

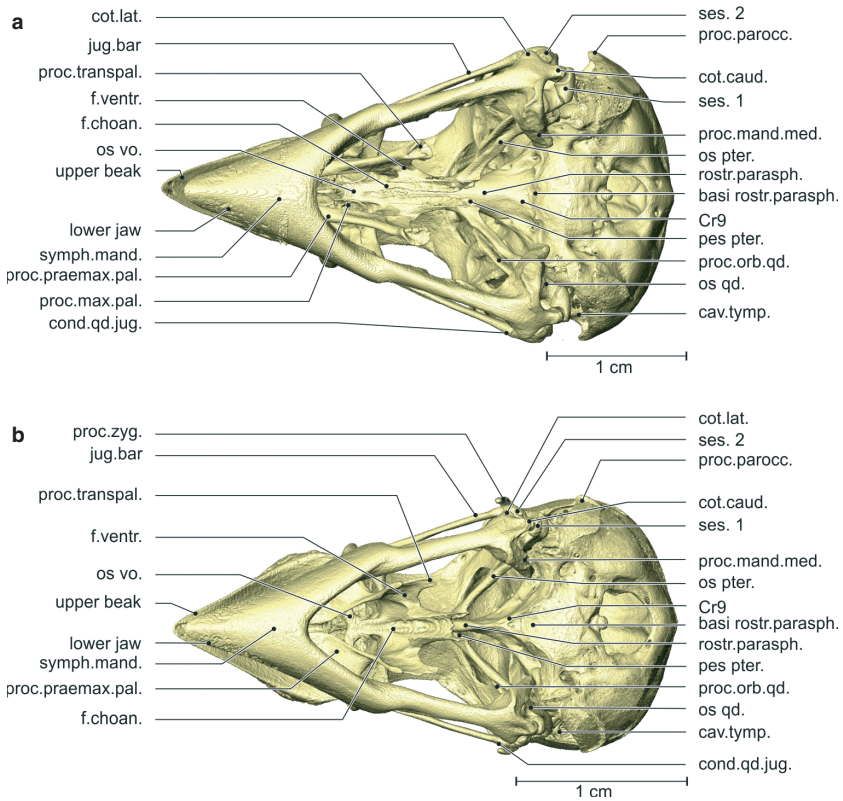

Fig. 3 Osteology. Ventral view of the skull of *Geospiza fortis* (a) and *Padda oryzivora* (b). Note that the os palatinum is more robust and narrower in *G. fortis*, and that the angle between the two rami of the lower jaw is greater. basi rostr.parasph., basi rostri parasphenoidalis; cav.tymp., cavum tympanicum; cond.qd.jug., condylus quadrati jugalis; cot.caud., cotyla caudalis; cot.lat., cotyla lateralis; f.choan., fossa choanalis; f.ventr., fossa ventralis; os pter., os pterygoideum; os qd., os quadratum; os vo., os vomer; pes pter., pes pteryoigei; proc.zyg., processus zygomaticus; proc.mand.med., processus mandibulae medialis; proc.max.pal., processus maxillae palatini; proc.orb.qd., processus orbitalis quadrati; proc.parocc., processus paroccipitalis; proc.praemax.pal., processus praemaxillae palatini; proc.transpal., processus transpalatinus; rostr.parasph., rostrum parasphenoidale; ses. 1, first sesamoid bone; ses. 2, second sesamoid bone; symph.mand., symphysis mandibulae.

ventrolateral side of the braincase is more oval instead of round.

Upper beak

Geospiza fortis (Figs 2–4). The upper beak is triangular and is comprised of three completely fused bones: the os nasale, the os praemaxillare and the rostral portion of the os maxillare. These three bones form the border of the nasal cavity in the caudal half of the upper beak. Dorsal in the nasal cavity, the laterally flattened and ventrocaudad facing nasal septum can be observed. The rostral portion of the os maxillare carries the caudomedially oriented flag-like processus palatinus maxillae, frequently referred to as the processus maxillopalatinus, a name that will be used here as well.

Ventrolaterally, the edges of the upper beak are formed by the two cristae tomialis. These cristae start at the rostral tip of the upper beak and run caudad to the processus maxillaris praemaxillae. Caudal to it lies the processus maxillaris nasalis, which is oriented slightly ventrocaudally.

The connections of the upper beak to the rest of the skull consist of flexion zones, characterized by a region of thin bone. A first flexion zone, the zona flexoria arcus jugalis, forms the connection between the upper beak and the jugal bar, ventrocaudal to the processus maxillaris praemaxillae and nasalis. Rostromedial to this connection, the upper beak connects to the os palatinum at the level of the zona flexoria palatina. This connection is bordered laterally by the long ventrocaudally pointing, slender processus palatinus praemaxillae. A third flexion zone, the zona flexoria arcus craniofacialis, also called the frontonasal hinge, is situated at the dorsocaudal side of the upper beak where it connects to the braincase.

Padda oryzivora (Figs 2–4). The upper beak is relatively broader. A larger part of the os maxillare is fused with the os praemaxillare before it continues into the jugal bar. The base of the processus maxillopalatinus is stronger and articulates with the lateral wings of the os vomer. The mediocaudally orientated flag-like plate of this process is almost absent. The processus palatinus praemaxillae could not be distinguished from the processus praemaxillaris palatini, which suggests that they may be fused, resulting in a much broader connection between the palatinum and the upper beak.

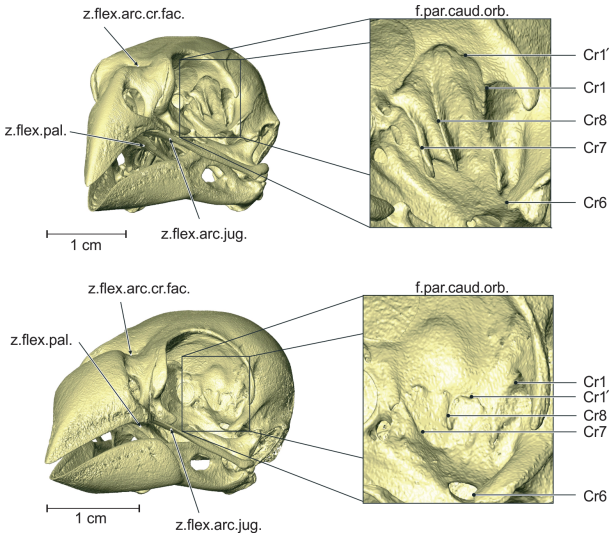

Fig. 4 Osteology. Rostrolateral view of the left side of the skull of *Geospiza fortis* (a) and *Padda oryzivora* (b) with detail of the fossa parietalis caudalis orbitalis. Note that the cristae in the fossa parietalis caudalis orbitalis are much more developed in *G. fortis*. f.par.caud.orb., fossa parietalis caudalis orbitalis; z.flex.arc.cr.fac., zona flexoria arcus cranio facialis; z.flex.arc.jug., zona flexoria arcus jugalis; z.flex.pal., zona flexoria palatine.

Palate

Geospiza fortis (Figs 2, 3 and 5). The palate is composed of the os palatinum and the os vomer, which are completely fused in the adult. The palate is connected to the upper beak, the os pterygoideum and the braincase, and can be divided into two parts: a pars choanalis and a pars lateralis.

The pars choanalis bears a paired lamella dorsalis, hence forming a U-shaped gutter surrounding the rostrum parasphenoidale. The facies articularis parasphenoidalis forms the contact zone between the lamella dorsalis and the rostrum parasphenoidale. Dorsally, the pars choanalis is bordered by the crista dorsolateralis, forming the dorsal edge of the lamella dorsalis. The lamella dorsalis articulates dorsocaudally with the pes pterygoidei of the os pterygoideum, through the facies articularis pterygoidei. This articulation is ventrally bordered by the caudally pointing processus pterygoidei. At its rostral side the pars choanalis is fused to the os vomer. It forms a rostrally orientated plate of which the rostrolateral tips are folded upwards, forming small lateral wings.

The pars choanalis has two ventral fossae: a fossa choanalis and a fossa ventralis. The fossa choanalis is positioned more medially and is bounded mediodorsally by the crista medialis, and ventrolaterally by the crista ventralis. This laterally orientated crista ventralis is well developed, bearing a sharp rostral tip. The second fossa, the fossa ventralis, lies at the ventromedial side of the pars lateralis and bridges the crista ventralis and the crista lateralis. The fossa is bordered rostrally by the angulus caudomedialis and caudally by the angulus caudolateralis.

The pars lateralis is largely comprised of the processus praemaxillaris palatini, which is a long, slender and slightly dorsoventrally flattened process, oriented rostrodorsomedially. It connects with the upper beak medial to the processus palatinus praemaxillae, where it forms the zona flexoria palatina. Further caudally, in line with the processus praemaxillaris palatini, the caudoventrally pointing processus

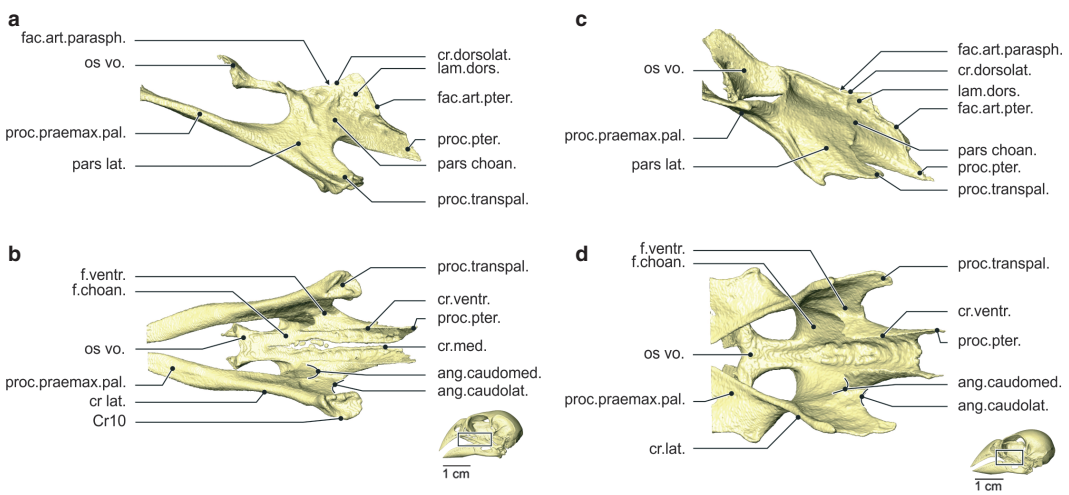

Fig. 5 Osteology. Lateral (a) and ventral (b) view of the os palatinum of *Geospiza fortis*, and lateral (c) and ventral (d) view of the os palatinum of *Padda oryzivora*. As already mentioned in Fig. 2, the wideness of the os palatinum is the biggest difference between both species studied. Also note the difference between the processus transpalatinus and os vomer. ang.caudolat., angulus caudolateralis; ang.caudomed., angulus caudomedialis; cr.ventr., crista ventralis; cr.dorsolat., crista dorsolateralis; cr.lat., crista lateralis; cr.med., crista medialis; fac.art.parasph., facies articularis parasphenoidalis; fac.art.pter., facies articularis pterygoidei; f.choan., fossa choanalis; f.ventr., fossa ventralis, lam.dors., lamella dorsalis; os vo., os vomer; pars choan., pars choanalis; pars lat., pars lateralis; proc.transpal., processus transpalatinus; proc.praemax.pal., processus praemaxillaris palatini; proc.pter., processus pterygoidei.

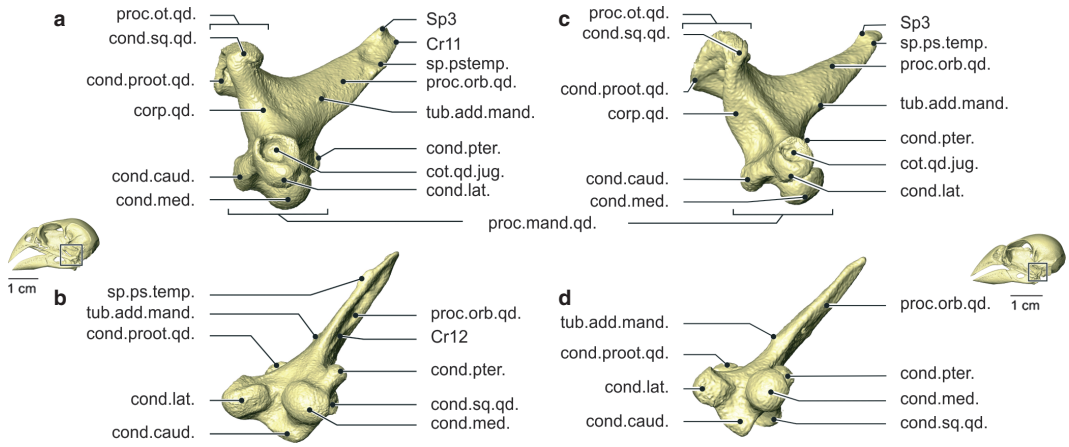

Fig. 6 Osteology. Lateral (a) and ventral (b) view of the right os quadratum of *Geospiza fortis*, and lateral (c) and ventral (d) view of the right os quadratum of *Padda oryzivora*. Note that the processus orbitalis is somewhat more robust in *G. fortis*, but that the ossa quadrata of these species are overall very similar. cond.caud., condylus caudalis; cond.lat., condylus lateralis; cond.med., condylus medialis; cond.proot.qd., condylus prooticus quadrati; cond.pter., condylus pterygoidei; cond.qd.jug., condylus quadrati jugalis; cond.sq.qd., condylus squamosus quadrati; corp.qd., corpus quadrati; proc.mand.qd., processus mandibularis quadrati; proc.orb.qd., processus orbitalis quadrati; proc.ot.qd., processus oticus quadrati; sp.ps.temp., spina pseudotemporalis; tub.add.mand., tuberculum adductor mandibulae.

transpalatinus can be observed. Ventrolaterally, the pars lateralis is bordered with the crista lateralis. The caudoventral edge of the processus transpalatinus is formed by an almost circular crista (Cr10), leaving a small depression in the middle.

Padda oryzivora (Figs 2, 3 and 5). Several differences can be observed in the structure of the palate. At the dorsalmost part of the facies articularis pterygoidei, the lamella dorsalis and the pes pterygoidei are fused. A crista medialis is absent because the left and right palatine bones are fully fused medially. The lateral wings of the os vomer are much more developed and articulate with the upper beak through the processus maxillopalatinus of the os maxillare. The pars lateralis is broader with a less prominent but more flattened processus transpalatinus. The processus praemaxillaris palatini is dorsoventrally flattened and oriented as if it has twisted 180 ° to the lateral. The connection of this process with the upper beak is much larger and takes up almost the entire width of the upper beak. The rostral tip of the crista ventralis is largely absent.

Os pterygoideum

Geospiza fortis (Figs 2 and 3). The os pterygoideum is a slender, elongated bone that forms the connection between the os quadratum and the os palatinum. The os pterygoideum can be divided into three parts: the pes pterygoidei, the corpus pterygoidei and the processus quadraticus pterygoidei. The dorsomedially situated pes pterygoidei forms the rostral expanded and mediolaterally flattened end. The pes pterygoidei articulates with the os palatinum at the level of its ventrorostral side, i.e. the facies articularis palatina. The medial side of the pes pterygoidei can shift along the rostrum parasphenoidale at the level of the facies articularis parasphenoidalis. The ventral end of facies articularis parasphenoidalis is slightly curved mediad, surrounding the ventral side of the rostrum parasphenoidale. Caudal to the facies articularis parasphenoidalis lies a distinct, ventrocaudad tuberculum.

The slender corpus pterygoidei is in cross-section triangular, but rounded at its caudal end near the processus quadraticus pterygoidei. This process articulates with the condylus pterygoidei of the os quadratum by means of a ball and socket joint. A small tubercle is situated on the dorsocaudal side of the process quadraticus, which probably reduces the degrees of freedom of this joint. Rostral to this process, on the dorsal side, a processus dorsalis points dorsomediorostrally, in line with the corpus pterygoidei.

Padda oryzivora (Figs 2 and 3). The pes pterygoidei is rostrodorsally fused with the os palatinum, and the ventral end does not surround the rostrum parasphenoidale. The processus dorsalis is smaller but still prominent, and the small tubercle at the dorsocaudal end of the processus quadraticus lies somewhat more laterally. In cross-section, the corpus pterygoidei is triangular but with more rounded angles.

Arcus jugale

Geospiza fortis (Figs 2 and 3). The jugal bar consists of three bones, i.e. the caudal portion of the os maxillare, the os jugale and the os quadratojugale, together forming a single mechanical unit. It is long and slender and originates just dorsal to the processus palatinus praemaxillae, and medioventral to the processus maxillaris praemaxillae and nasalis. It runs laterocaudad to end in the condylus quadrati jugalis, which has two articulation facets: a dorsal facet, of

which the tip is slightly rotated medially; and a smaller facet, ventrorostrally to the first one and facing caudally. The dorsal facet fits into the cotyla quadratojugalis of the os quadratum, while the ventral facet rests on the rostral edge of this cotyla. The caudal half of the jugal bar is flattened mediolaterally, apart from the condyle, whereas the rostral half is flattened dorsoventrally. A spine is situated at the dorsal side in the transition zone between the os maxillare and the os jugale, pointing rostrally, in line with the jugal bar.

Padda oryzivora (Figs 2 and 3). The condylus quadrati jugalis is somewhat smaller and the dorsal spine is absent. Instead, a small dorsomedial crista is present.

Os quadratum

Geospiza fortis (Figs 2, 3 and 6). The os quadratum forms the link between the jugal bar, the os pterygoideum, the lower jaw and the braincase. It roughly has the shape of a tetrahedron, with the four tips represented rostromedially by the processus orbitalis quadrati, dorsocaudally by the processus oticus quadrati, ventrolaterally by the condylus lateralis and the cotyla quadratojugalis of the processus mandibularis quadrati, and ventromedially by the condylus medialis, the condylus pterygoideus and the condylus caudalis of the processus mandibularis quadrati.

The rostral-most process of the os quadratum, the processus orbitalis quadrati, is a long, mediolaterally flattened process pointing mediorostrodorsally. The ventral end of its distal tip is turned slightly medially, while the dorsal end is rotated slightly laterally. The process contains three small protrusions. A first small tubercle, the tuberculum adductor mandibulae, is situated laterally at the base of the process. A second spine, the spina pseudotemporalis, is positioned lateroventrally, just proximal to the distal end of the process. A third spine (Sp3) is situated dorsally at the distal tip of the process. The rostrolateral end of the process has a small fossa that is rostrally bordered by a prominent crista (Cr11), running from the spina pseudotemporalis over the distal tip of the process to the dorsal Sp3. Along the medial side of the process, another fossa is situated, dorsally bordered by a crista (Cr12).

The processus oticus quadrati bears two articulations with the braincase. The medial facet, the condylus prooticus quadrati, is supported by a ventrorostrolateral pila, connecting the condyle to the corpus quadrati. The second facet, the condylus squamosus quadrati, is situated rostrolaterally of the condylus prooticus quadrati. The condylus squamosus quadrati is connected to the corpus quadrati by a ventrocaudomediad pila, running rostromedially from that of the condylus prooticus quadrati. The condylus prooticus quadrati has a round articulation facet, while the articulation facet of the condylus squamosus quadrati is slightly oval.

The third process of the os quadratum is the processus mandibularis quadrati, and is comprised of four condyles. The condylus medialis is situated medioventrally and has the largest articulation surface. It articulates ventrally with the cotyla medialis of the lower jaw, in which it can slide or rotate. The smallest condylus pterygoideus of the processus mandibularis quadrati lies rostrally to the condylus medialis and medioventrally to the processus orbitalis quadrati. This condyle articulates with the processus quadraticus of the os pterygoideum. The most lateral condylus lateralis carries the cotyla quadratojugalis rostrolaterally, which articulates with the proximal end of the jugal bar. Its rostral edge forms a surface on which the jugal bar rests. The condylus lateralis itself articulates ventrally with the dorsal surface of the cotyla lateralis of the processus mandibulae lateralis. It has an oval articulation head, which is slightly oriented caudally. Caudally to this articulation lies a small sesamoid bone (ses. 2). In between and dorsocaudally to the condylus lateralis and the condylus medialis lies the fourth condyle, i.e. the condylus caudalis, which articulates with the cotyla caudalis of the processus mandibulae lateralis through a second and larger sesamoid bone (ses. 1). In previous studies, these small particles are called menisci articularis. However, these parts are made up of bony tissue, instead of cartilage as is the case in a meniscus. Also, they are formed inside a ligament (see below), a feature characterizing sesamoid bones. As such, we consider it more suitable to refer to these particles as sesamoid bones. Jollie (1957) also mentioned these two additional bones ('ossicula articularia') lying in the posterior wall of the articular capsule of the quadrate-mandibular joint in several birds. Nuijens & Zweers (1997) only found one in the greenfinch and the spice finch.

Padda oryzivora (Figs 2, 3 and 6). At first sight the os quadratum of *P. oryzivora* resembles that of *G. fortis*, apart from some small differences. The lateral fossa and Cr11 of the processus orbitalis quadrati are markedly less prominent. The spina pseudotemporalis, the medial fossa and Cr12 of the processus orbitalis quadrati are largely absent. The condylus proöticus quadrati of the processus oticus quadrati and the condylus lateralis of the processus mandibulae lateralis are somewhat smaller. The condylus squamosus quadrati is slightly more elongated and the ventral head of the condylus lateralis quadrati is orientated more rostrally.

Lower jaw

Geospiza fortis (Figs 2, 3 and 7). All elements that make up the lower jaw are fully fused in an adult *G. fortis*. The rostral part of each ramus is the pars dentalis, which has a triangular shape. In the rostral two-thirds of this part, i.e. the rostrum mandibulae, the two mandibular rami are completely fused ventrally and form a strong symphysis mandibularis. The cristae tomialis form the dorsal edges of the rami

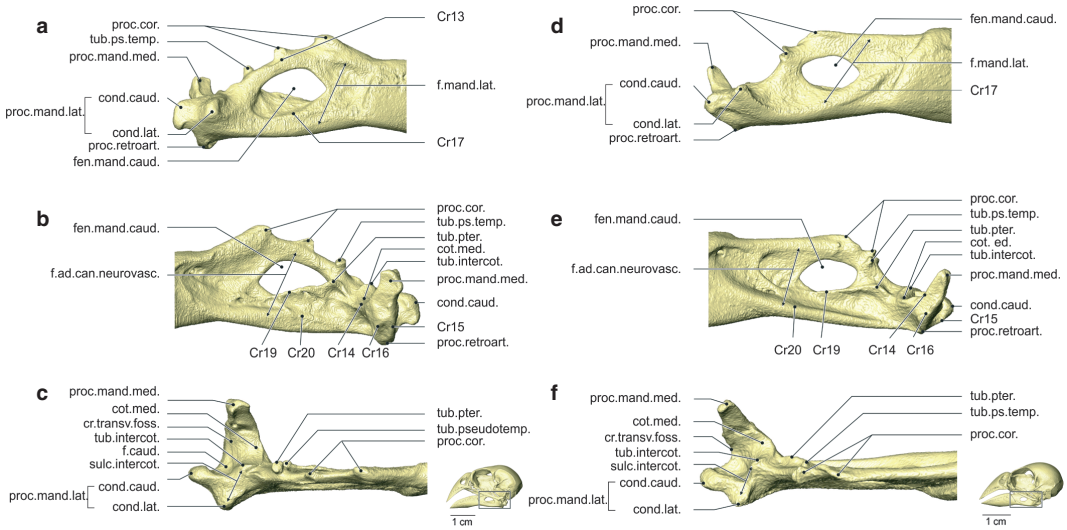

Fig. 7 Osteology. Lateral (a), medial (b) and dorsal (c) view of the pars caudalis of the mandibula (right) of *Geospiza fortis*, and lateral (d), medial (e) and dorsal (f) view of the pars caudalis of the mandibula (right) of *Padda oryzivora.* Note the prominent processus coronoideus with two well-developed tubercles in *G. fortis*, and the big difference in position of the tuberculus pseudotemporalis between both species. cond.caud., condylus caudalis; cond.lat., condylus lateralis; cot.med., cotyla medialis; cr.transv.f., crista transversa fossae; fen.mand.caud., fenestra mandibulae caudalis; f.ad.can.neurovasc., fossa aditus canalis neurovascularis; f.caud., fossa caudalis; f.mand.lat., fossa mandibulae lateralis; proc.cor., processus coronoideus; proc.mand.lat., processus mandibulae lateralis; proc.mand.med., processus mandibulae medialis; proc.retroart., processus retroarticularis; sulc.intercot., sulcus intercotylaris; sub.intercot., tuberculum intercotylaris; tub.ps.temp., tuberculum pseudotemporalis; tub.pter., tuberculum pterygoideum.

and run from the rostral tip of the lower jaw to the end of the pars dentalis.

The caudal part of the lower jaw is called the pars caudalis, which is characterized by four processes: the processus coronoideus, mandibulae medialis, mandibulae lateralis and retroarticularis. The two tubercles are at the dorsal edge of the pars caudalis or situated on the processus coronoideus. The rostral tubercle points dorsally. The second tubercle points dorsocaudally with a curved crista (Cr13) running along its lateral side. A second process of the lower jaw, the processus mandibulae lateralis, is formed by two merged articulation facets: the cotyla lateralis and the cotyla caudalis. The two cotylae are part of the fossa articularis quadratica, where the lower jaw articulates with the os quadratum, articulating, respectively, with the condylus lateralis and the condylus caudalis of the processus mandibularis quadrati. This fossa comprises a third articulation facet, the cotyla medialis, which articulates with the condylus medialis of the os quadratum. It is separated from the cotyla lateralis by the sulcus intercotylaris. Lateral to the cotyla medialis, at the medial side of the sulcus intercotylaris, lies the dorsal tuberculum intercotylare. The long and slender processus mandibulae medialis points dorsomedially. Four cristae run along this process. The first crista (Cr14) forms the rostral margin of the process running along the rostral edge of cotyla medialis to end in the tuberculum pterygoidei (new term). A second, curved crista (Cr15) forms the caudal margin of the process and runs to the base of the condylus caudalis of the processus mandibulae lateralis. This crista runs ventrally over the poorly developed fourth processus retroarticularis. The third and curved crista transversa fossae runs from the medial side of the processus medialis to the lateral side of the condylus caudalis. These second and third cristae enclose the fossa caudalis. The fourth and last crista (Cr16) lies at the medioventral side of the process.

The fenestra mandibulae caudalis is situated centrally in the pars caudalis. At the lateral surface of the pars caudalis a crista (Cr17) borders the fenestra mandibulae caudalis ventrally. The fossa mandibulae lateralis is present on the lateral side of the pars caudalis as a large but shallow cavity. At the medial side, the pars caudalis has two cristae, two tubercles and a fossa. The tuberculum pseudotemporalis is a well-developed mediodorsally orientated tubercle, which is situated caudally to the second tubercle of the processus coronideus. The tuberculum pterygoidei is small and situated ventromedially of the tuberculum pseudotemporalis. The ventral margin of the fenestra mandibulae caudalis is formed by a prominent crista (Cr19), running rostroventrally from the base of the tuberculum pterygoidei. The second crista (Cr20) runs from the rostral margin of the pars caudalis to the base of the processus mandibulae medialis and forms the ventral margin of the fossa aditus canalis neurovascularis.

Padda oryzivora (Figs 2, 3 and 7). The caudal portion of the pars dentalis is relatively higher. The processus coronoideus is positioned more caudally, is relatively less high and

the second tubercle is divided into two small spines; one is positioned rostrodorsally and one laterodorsally. The tuberculum pseudotemporalis is much smaller and lies medially of the second tubercle of the processus coronoideus. Rostral to the fenestra mandibulae caudalis, a depression with a distinct rostral and rostroventral border can be observed. The shape of processus mandibulae medialis, lateralis and retroarticularis is similar to that of *G. fortis*, although less robust and the processus mandibulae medialis is oriented somewhat more caudally.

Ligaments

Geospiza fortis (Figs 8 and 9). Two ligaments reinforce the quadratomandibular and quadrate-quadratojugal joints. The first strong ligament, i.e. the ligamentum jugomandibulare mediale, bridges the lateral and caudal parts of the quadratomandibular and the quadrate-quadratojugal joints, and consists of two parts. The lateral part originates on the ventrocaudal edge of the rostral articulation facet of the condylus quadrati jugalis and runs caudally to insert on the biggest sesamoid bone (ses. 1). The second, smaller sesamoid bone (ses. 2) can be found in the center of this part of the ligament. The caudomedial part of the ligament is shorter and originates at the medial side of the big sesamoid, running medially to insert on the crista transversa fossae, on the lateral side of the processus mandibulae medialis. In addition to the ligamentum jugomandibulare mediale, the ligamentum jugomandibulare laterale also holds the quadrate-quadratojugal articulation in place. This short and small ligament connects the jugal bar to the lower jaw. It originates laterally on the tip of the condylus quadrati jugalis and inserts just in front of the quadratomandibular joint, rostral to the condylus lateralis of the processus mandibularis lateralis. The ligament covers the lateral part of the ligamentum jugomandibulare mediale.

The articulation between the os palatinum, os pterygoideum and the rostrum parasphenoidale is bridged by the large ligamentum mesethmopalatinum. It attaches on the crista dorsolateralis of the os palatinum and the dorsal edge of the os pterygoideum, and forms a firm connection between the caudal edge of the lamella dorsalis of the os palatinum and the rostral edge of the pes pterygoidei. The ligament inserts on the septum interorbitale, just dorsal to the articulation of the os palatinum and os pterygoideum with the rostrum parasphenoidale. The cristae medialis of the left and right palatine bones are connected through the ligamentum interpalatinum (new term).

The ligamentum occipitomandibulare connects the cranium with the lower jaw. It starts at the proximal and ventral border of the processus paroccipitalis, dorsal to the aponeurosis 1 of musculus depressor mandibulae, and runs rostrally to insert on the processus medialis mandibulae. The insertion lies dorsomedial to the insertion of the ligamentum jugomandibularis medialis on the crista transversa fossae of the processus medialis mandibulae.

Two ligaments hold the os quadratum in position to the cranium. The ligamentum quadratosphenoidale runs from the caudomedial side of the os quadratum to the os parasphenoidale, whereas the ligamentum quadratotemporale runs from the dorsolateral side of the processus oticus quadrati to the processus suprameaticus.

Padda oryzivora (Figs 8 and 10). A ligamentum postorbitale is found. It is a strong and long ligament that connects the processus postorbitalis with the lower jaw and runs external to the quadrate-quadratojugal articulation. The ligament originates at the distal tip of the processus postorbitalis and inserts just before the quadratomandibular joint on the rostral edge of the condylus lateralis of the processus mandibularis lateralis. The ligamentum jugomandibulare laterale runs over this ligament at its place of insertion and inserts just ventral to it.

As the pes pterygoidei and the os palatinum are dorsally fused, the ligamentum mesethmopalatinum does not need to reinforce this connection and only attaches on the crista dorsolateralis of the os palatinum and on the dorsal edge of the os pterygoideum, and inserts on the septum interorbitale.

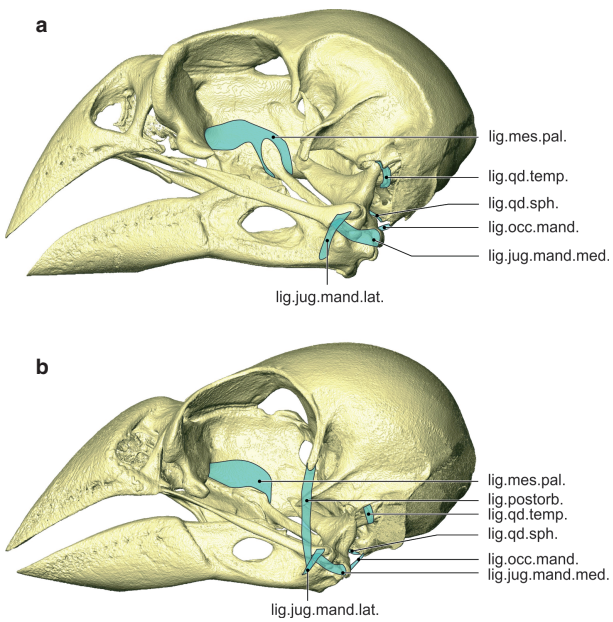

Fig. 8 Ligaments. Lateral view of the left side of the skull of *Geospiza fortis* (a) and *Padda oryzivora* (b) showing the ligaments. Note the absence of the ligamentum postorbitalis in *G. fortis*. Also note the difference in the ligamentum mesethmopalatinum in *G. fortis*, which connects the os palatinum with the pes pterygoidei. lig.jug.mand.lat., ligamentum jugomandibulare laterale; lig.jug.mand.med., ligamentum jugomandibulare mediale; lig.mes.pal., ligamentum mesethmopalatinum; lig.occ.mand., ligamentum occipitomandibulare; lig.postorb., ligamentum postorbitale; lig.qd.sph., ligamentum quadratosphenoidale; lig.qd.temp., ligamentum quadratotemporale.

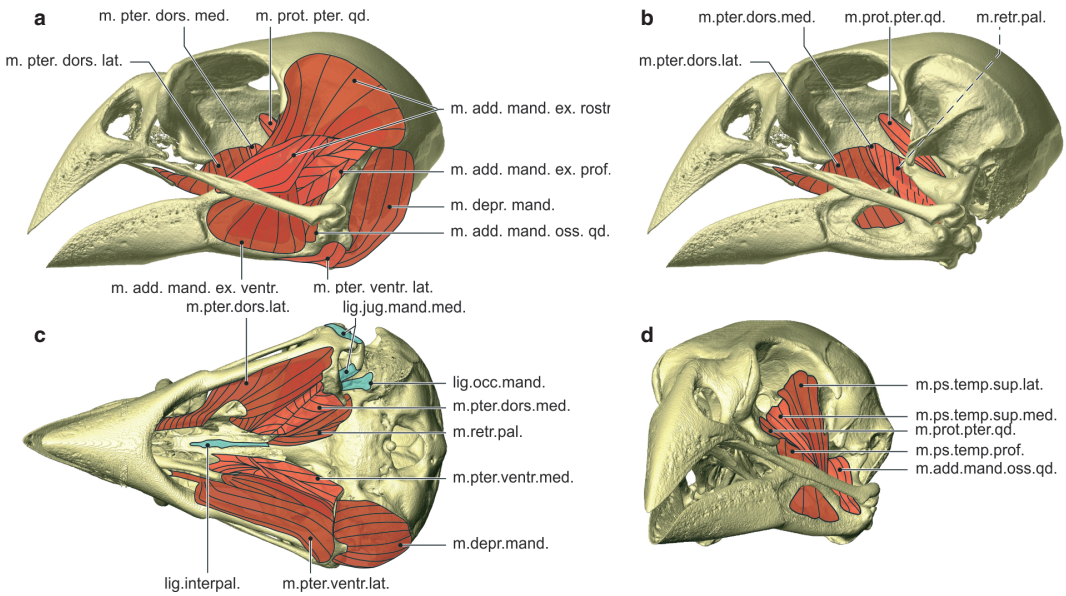

Fig. 9 Myology *Geospiza fortis*. Lateral view of the skull showing the lateral muscles (a), lateral view of the skull showing the medial muscles (b), ventral view of the skull showing the ventral muscles and ligaments, with the most ventral muscles on the left side of the skull and the most dorsal muscles on the right side of the skull (c), and rostrolateral view of the skull showing the pseudotemporal muscles and the musculus adductor mandibulae ossis quadrati and the musculus protractor pterygoidei et quadrati (d). lig.interpal., ligamentum interpalatinum; lig.jug.mand.med., ligamentum jugomandibulare mediale; lig.occ.mand., ligamentum occipitomandibulare; m.add.mand.ex.rostr., musculus adductor mandibulae externus rostralis; m.add.mand.ex.ventr., musculus adductor mandibulae externus ventralis; m.add.mand.ext.prof., musculus adductor mandibulae externus profundus; m.add.mand.oss.qd., musculus adductor mandibulae ossis quadrati; m.depr.mand., musculus depressor mandibulae; m.prot.pter.qd., musculus protractor pterygoidei et quadrati; m.ps.temp.sup.lat., musculus pseudotemporalis superficialis lateralis; m.ps.temp.sup.med., musculus pseudotemporalis superficialis medialis; m.pter.dors.lat., musculus pterygoideus dorsalis lateralis; m.pter.dors.med., musculus pterygoideus dorsalis medialis; m.pter.ventr.lat., musculus pterygoideus ventralis lateralis; m.pter.ventr.med., musculus pterygoideus ventralis medialis; m.retr.pal., musculus retractor palatini.

The ligament interpalatinum is absent as the left and right palatine bones are fused.

Myology

Statistical results

The MANOVA testing for differences in fiber length was significant (Wilks' lambda = 0.001; $F_{4,1}$ = 525.79; P = 0.033), with *G. fortis* having slightly longer fibers in the m. pseudotemporalis and the m. pterygoideus ventralis than *P. oryzivora*. Although a MANOVA testing for differences in muscle mass detected no overall differences (Wilks' lambda = 0.034; $F_{4,1}$ = 7.21; P = 0.27), subsequent univariate ANOVAs demonstrated that differences in the mass of the external adductors ($F_{1,4}$ = 18.27; P = 0.013), the m. pseudotemporalis ($F_{1,4}$ = 31.82; P = 0.005) and the m. pterygoideus ($F_{1,4}$ = 24.32; P = 0.008) exist, but in not the m. retractor palatini ($F_{1,4}$ = 7.25; P = 0.06), with *G. fortis* having bigger jaw muscles than *P. oryzivora*. Similarly, although the MANOVA testing for overall differences in PCSA was not significant (Wilks' lambda = 0.007; $F_{4,1}$ = 37.52; P = 0.12), differences in the cross-sectional area of the m. pseudotemporalis ($F_{1,4}$ = 25.03; P = 0.007) and the m. retractor palatini ($F_{1,4}$ = 9.11; P = 0.04) were significant. Although cross-sectional areas were larger for *G. fortis* for the other muscle groups, they were not significantly so (external adductor: $F_{1,4}$ = 6.13; P = 0.069; m. pterygoideus: $F_{1,4}$ = 7.52; P = 0.052). Differences between species in bite force were highly significant ($F_{1,4}$ = 286.87; P < 0.001). As the mass of the muscles in *G. fortis* is generally greater than that of the jaw muscles in *P. oryzivora*, such differences in muscle size will not be further described in the comparison between both species. Below we thus provide only a qualitative description of the origin and insertion of the muscles and their type of pennation.

Musculus depressor mandibulae

Geospiza fortis (Fig. 9). The musculus depressor mandibulae connects the braincase with the lower jaw. Its parallel oriented fibers originate at the processus paroccipitalis, with the ventral part of the crista temporalis forming the dorsal border and the crista transversa nuchalis forming the caudal border. On the rostral edge of the processus paroccipitalis inserts a short but broad aponeurosis (Ap1) that forms the medial surface of the muscle, with fibers only attaching on the lateral side of the aponeurosis. The muscle inserts on the fossa caudalis of the lower jaw between the crista transversa fossae and Cr15. This insertion is ventrally

bordered by a second, larger aponeurosis (Ap2), which inserts on Cr15.

Padda oryzivora (Fig. 10). No differences were observed.

Musculus adductor mandibulae externus rostralis

Geospiza fortis (Fig. 9). Two parts can be distinguished in the musculus adductor mandibulae externus rostralis. The dorsal and biggest part inserts on the anterior tubercle of the processus coronoideus, and extends dorsocaudally to fill up the fossa temporalis on the cranium. Its attachment is bordered ventrally by Cr3, dorsocaudally by the crista temporalis and rostromedially by Cr1. A large aponeurosis (T-Ap1) originates inside the muscle, with muscle fibers attaching to both sides of the aponeurosis, and converges into a thick tendon that attaches to the most rostral part of the processus coronoideus. At its lateroventral side, the aponeurosis has a small wing-like extension that is oriented mediolaterally. The dorsal side of this wing-like extension serves as an attachment site for muscle fibers of the dorsal part of this muscle, while fibers from the much smaller ventral part (discussed below) attach on the ventral side hereof. The muscle is laterally bordered by a second clear aponeurosis (Ap2), which attaches to the crista temporalis and forms the external surface of the muscle. A third aponeurosis (Ap3) runs through the medial part of this muscle, and lies between the processus postorbitalis and zygomaticus. Its dorsal edge connects to the medial edge of T-Ap1. This medial part is medially bordered by an aponeurosis (Ap4) to which fibers attach at its lateral side only. This aponeurosis is divided in two parts and inserts on the braincase on Cr1. Another, very small tendon (T5) lies laterally to Ap4 and attaches to the processus coronoideus, just caudal to the attachment of T-Ap1.

The ventral, much smaller part lies ventral to the first part. It originates on Cr4 of the processus zygomaticus, thereby covered by the dorsal part of this muscle and attaching to the ventral surface of the wing-like extension of T-Ap1. Anteriorly, it inserts on the dorsolateral edge of the lower jaw, rostral to the processus coronoideus, thereby covering the tendon (T-Ap3) of the musculus adductor mandibulae externus ventralis, on which its medial fibers attach. Two tendons are present. A first, rostral tendon (T6) inserts just rostral to T-Ap1 on the dorsolateral edge of the lower jaw. The second, proximal tendon (T7) attaches to Cr4 on the processus zygomaticus.

Padda oryzivora (Fig. 10). The origin of the dorsal part of the musculus adductor mandibulae externus rostralis on the braincase does not extend as far dorsal on the cranium compared with *G. fortis*.

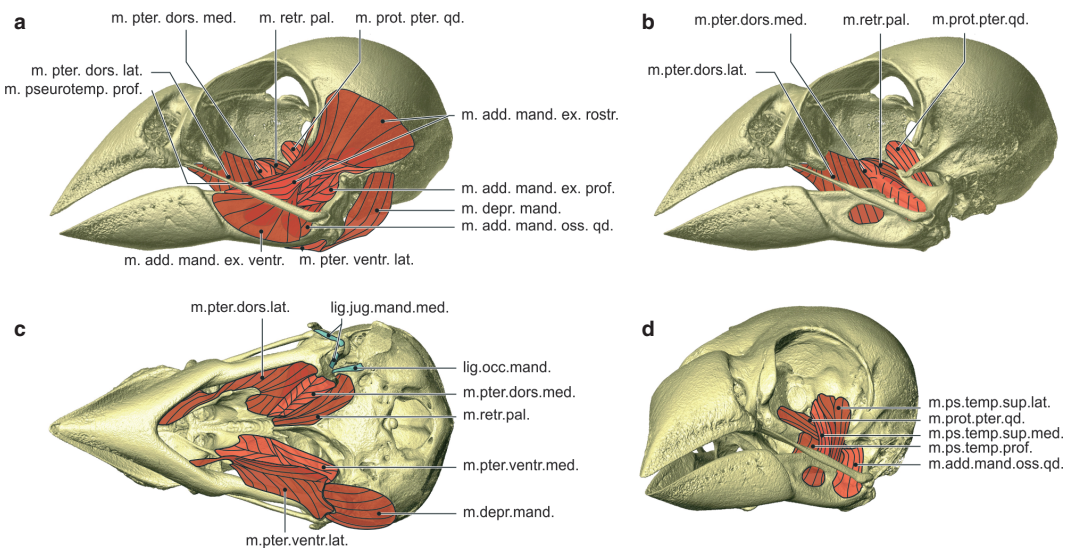

Fig. 10 Myology *Padda oryzivora*. Lateral view of the skull showing the lateral muscles (a), lateral view of the skull showing the medial muscles (b), ventral view of the skull showing the ventral muscles and ligaments, with the most ventral muscles on the left side of the skull and the most dorsal muscles on the right side of the skull (c), and rostrolateral view of the skull showing the pseudotemporal muscles and the musculus adductor mandibulae ossis quadrati and the musculus protractor pterygoidei et quadrati (d). lig.interpal., ligamentum interpalatinum; lig.jug.mand.med., ligamentum jugomandibulare mediale; lig.occ.mand., ligamentum occipitomandibulare; m.add.mand.ex.rostr., musculus adductor mandibulae externus rostralis; m.add.mand.ex.ventr., musculus adductor mandibulae externus ventralis; m.add.mand.ext.prof., musculus adductor mandibulae externus profundus; m.add.mand.oss.qd., musculus adductor mandibulae ossis quadrati; m.depr.mand., musculus depressor mandibulae; m.prot.pter.qd., musculus protractor pterygoidei et quadrati; m.ps.temp.sup.lat., musculus pseudotemporalis superficialis lateralis; m.ps.temp.sup.med., musculus pseudotemporalis superficialis medialis; m.pter.dors.lat., musculus pterygoideus dorsalis lateralis; m.pter.dors.med., musculus pterygoideus dorsalis medialis; m.pter.ventr.lat., musculus pterygoideus ventralis lateralis; m.pter.ventr.med., musculus pterygoideus ventralis medialis; m.retr.pal., musculus retractor palatini.

Musculus adductor mandibulae externus ventralis

Geospiza fortis (Fig. 9). The triangular ventral part of the musculus adductor mandibulae externus originates on Cr5 of the processus zygomaticus, rostroventral to the origin of the ventral part of the musculus adductor mandibulae externus rostralis. Its fibers insert fanlike on the lateral surface of the lower jaw, filling up the fossa mandibulae lateralis and covering the fenestra mandibulae caudalis. The muscle is covered laterally by the jugal bar and the glandula mandibularis externa (external salivary gland), which leave an impression in the muscle. The ventromedial and ventrolateral sides of the muscle are bordered by aponeuroses (Ap1 and Ap2) that attach to the lower jaw, ventral to the fenestra mandibulae caudalis. A third and much larger aponeurosis (T-Ap3) originates inside the muscle and converges into a thick tendon that inserts on Cr5 of the processus zygomaticus. Muscle fibers insert on this aponeurosis on both sides, with more fibers attaching on the medial side.

Padda oryzivora (Fig. 10). The aponeuroses Ap2 and Ap3 are very thin and difficult to observe.

Musculus adductor mandibulae externus profundus

Geospiza fortis (Fig. 9). The musculus adductor mandibulae externus profundus caudally fills up the ventral part of the fossa temporalis on the cranium. It is bordered ventrally by Cr3 and dorsally by the processus zygomaticus and Cr4. The muscle runs rostroventrally and inserts on the second tubercle of the processus coronoideus of the lower jaw. It is a very thick, short and multipennate muscle with a complex web of aponeuroses. Seven aponeuroses can be distinguished, which will be numbered from lateral to medial. The first aponeurosis (Ap1) is short and inserts on the caudal half of Cr4 of the processus zygomaticus. The second aponeurosis covers the lateral and ventral surface of the muscle and attaches to the lateral part of the second tubercle of the processus coronoideus. Rostromedial to the attachment of the Ap2, on the dorsal surface of the second tubercle of the processus coronoideus, inserts a third and long aponeurosis (Ap3), which runs almost through the whole muscle. The fourth aponeurosis (Ap4) is actually a collection of five parts that run parallel to each other and originate on Cr3, dorsal to the quadrato-squamoso-otical joint. The aponeuroses are all small, with parts 1, 3 and 5 (from dorsal to ventral) being the biggest, and parts 2 and 3 being only very small strands. Ventromedial to Ap4 inserts a fifth, small aponeurosis (Ap5), just dorsal to the quadrato-squamoso-otical joint. The sixth and seventh aponeuroses (Ap6 and Ap7) both insert on the second tubercle of the processus coronoideus just medial to the Ap3. Ap7 is the most medial aponeurosis and forms the medial surface of the musculus adductor mandibulae externus profundus.

Padda oryzivora (Fig. 10). Partly due to the difference in the shape of the processus coronoideus and the presence of a tuberculum squamosum, some differences can be noted. Ap1 is much larger and covers the total lateral surface of the caudal part of the musculus adductor mandibulae externus profundus. Ap2 attaches to the rostrodorsal spine of the second tubercle of the processus coronoideus, and is folded with one part oriented mediolaterally and one part oriented dorsoventrally. Ap3 inserts on the laterodorsal and rostrodorsal spine of the second tubercle of the processus coronoideus, caudal to the attachment of Ap2. Ap4 consists only of two parts that insert on the tuberculum squamosum and the Cr3, respectively. Both aponeurosis are small and run parallel to each other. Ap5 is broader. Ap6 and Ap7 insert behind the rostrodorsal spine and medial to the laterodorsal spine of the second tubercle of the processus coronoideus, medial to the Ap3.

Musculus adductor mandibulae ossis quadrati

Geospiza fortis (Fig. 9). The parallel-fibered musculus adductor mandibulae ossis quadrati has its origin on the proximal part of the lateral as well as the medial surface of the processus orbitalis of the os quadratum. A first aponeurosis (Ap1) attaches to the tuberculum adductor mandibulae. The muscle runs rostroventrally to insert on the lateral and dorsal surface of the lower jaw, between the fenestra mandibulae caudalis and the processus mandibulae lateralis. A second aponeurosis (Ap2) inserts here on the rostrodorsal side of the condylus lateralis of the processus mandibulae lateralis. The musculus adductor mandibulae externus profundus and the musculus adductor mandibulae externus ventralis cover this muscle almost completely.

Padda oryzivora (Fig. 10). Some differences can be found at the level of the aponeuroses inserting on the os quadratum. In addition to Ap1, a second aponeurosis (Ap3) inserts on the proximal end of the processus orbitalis and forms the dorsal surface of the muscle. Ap2 is absent.

Musculus pseudotemporalis superficialis lateralis

Geospiza fortis (Fig. 9). The multipennate musculus pseudotemporalis superficialis lateralis runs from the caudal wall of the orbit to the lower jaw. It originates in the fossa parietalis orbitalis caudalis and attaches to the tuberculum pseudotemporalis. Two aponeuroses (Ap1 and Ap2) run through the entire muscle and attach on the tuberculum pseudotemporalis, on its lateral and dorsal side and on its caudolateral side, respectively, as well as on Cr8 and Cr1, respectively, of the fossa parietalis orbitalis caudalis. In that way, they act more like a ligament than as an aponeurosis. Ap1 not only runs to Cr8 but also covers the lateral and dorsal surface of the distal part of the muscle. Ap2 inserts medioventral to Ap4 of the musculus adductor mandibulae externus rostralis. A third aponeurosis (Ap3) attaches to the

dorsal crista of the fossa parietalis caudalis orbitalis and forms the dorsal surface of the dorsocaudal end of the muscle. The ventromedial muscle fibers also attach to the lateral side of Ap1 of the musculus pseudotemporalis superficialis medialis.

Padda oryzivora (Fig. 10). Ap1 and Ap2 do not run through the entire muscle but are both divided in two, with a rostral and caudal part. The rostral part of Ap1 attaches rostral to the tuberculum pseudotemporalis.

Musculus pseudotemporalis superficialis medialis
Geospiza fortis (Fig. 9). The medial part of the musculus pseudotemporalis superficialis originates on Cr7 in the fossa parietalis orbitalis caudalis and runs rostrolaterally to insert on the medial side of the lower jaw, just rostral to and on the rostral side of the tuberculum pseudotemporalis. Two aponeuroses (Ap1 and Ap2) enclose the muscle and run from the braincase to the lower jaw. Ap1 originates on Cr7 and runs rostrolaterally to insert on the rostral side of the tuberculum pseudotemporalis. It forms the lateral surface of the muscle. Some muscle fibers of the musculus pseudotemporalis superficialis lateralis attach to this aponeurosis. The second aponeurosis (Ap2) originates ventrocaudal to foramina nervus opticus and attaches just rostral to the tuberculum pseudotemporalis on the medial side of the lower jaw. The muscle fibers run from rostrolateral on Ap2 to insert mediocaudal on Ap1.

Padda oryzivora (Fig. 10). The insertion sites of the aponeuroses differ. Ap1 only inserts on Cr7 and does not reach to the lower jaw. Ap2 inserts as a broad sheet on the medial side of the lower jaw, dorsal to the fenestra caudalis mandibulae and the insertion of the musculus pseudotemporalis profundus, but does not insert on the braincase.

Musculus pseudotemporalis profundus
Geospiza fortis (Fig. 9). The broad musculus pseudotemporalis profundus runs rostrolaterally from the processus orbitalis of the os quadratum to the medial surface of the lower jaw. The muscle originates at the distal two-thirds of the processus orbitalis of the os quadratum, medially to the origin of the musculus adductor mandibulae ossis quadrati. Its place of origin is medially bordered by Cr11 and ventromedially by Cr12. Muscle fibers insert on the fossa aditus canalis neurovascularis, from anterior to the caudal edge of the rhamphotheca over the fenestra mandibulae caudalis to just rostral to the quadratomandibular joint. Muscle fibers insert on the lateral side of Cr19 and reach through the fenestra mandibulae caudalis to Cr17. Five aponeuroses could be observed, of which three insert on the processus orbitalis and two on the lower jaw. A first aponeurosis (Ap1) inserts on Sp3 at the distal end of the processus orbitalis and attaches to the dorsal and medial side of the lower jaw, caudal to the insertion of T6 of the musculus adductor mandibulae externus rostralis. The second aponeurosis (Ap2) inserts on Cr11 on the distal end of the processus orbitalis. Muscle fibers attach to both sides of this aponeurosis. The third aponeurosis (Ap3) inserts on the medial side of the first tubercle of the processus coronoideus and forms the lateral surface of the rostral part of the muscle. On the rostral edge of the processus orbitalis of the os quadratum inserts a fourth aponeurosis (Ap4) as a large sheet that runs rostrolaterally. The last aponeurosis (Ap5) is a very thin aponeurosis, almost invisible, that forms the lateral surface of the rostral part of the muscle and inserts on Cr19.

Padda oryzivora (Fig. 10). Some differences could be observed. Ap1 runs rostrolaterally to the lower jaw but does not attach to it. Ap3, Ap4 and Ap5 were absent or could not be found.

Musculus pterygoideus ventralis lateralis
Geospiza fortis (Fig. 9). The musculus pterygoideus ventralis lateralis is a large muscle running from the processus transpalatinus of the os palatinum to the lower jaw. Two parts can be distinguished. The dorsal part originates on the rostral half of Cr10 of the processus transpalatinus and runs laterocaudally. The fibers of the ventral part originate more rostrally with a long tendon (T-Ap1), which inserts on the processus palatinus praemaxillae but originates as a long, broad aponeurosis inside the muscle. The muscle inserts on the ventral side of the processus mandibulae medialis on Cr16, and on the ventral and ventromedial side of the pars caudalis of the lower jaw. Apart from the long T-Ap1, two other aponeuroses could be observed. The ventral surface of the muscle is bordered by an aponeurosis (Ap2), which inserts on the ventral surface of the lower jaw. A third, ligamentous aponeurosis (Ap3) connects the processus transpalatinus to the lower jaw, as its rostral end has a broad insertion on the rostral half of Cr10 of the processus transpalatinus and the lateral border of this aponeurosis runs to the processus mandibulae medialis where it inserts on Cr16. Dorsally the muscle is bordered by Ap1 of the musculus pterygoideus dorsalis lateralis. Muscle fibers are rostrocaudally oriented.

Padda oryzivora (Fig. 10). The dorsal part of the muscle also attaches on the processus transpalatinus, but fills up the lateral part of the fossa ventralis. The fibers from the dorsal part stop at the processus transpalatinus, and only T-Ap1 runs more rostrally, over the crista lateralis of the os palatinum, to insert on the lateral part of the processus praemaxillaris palatini. Also in the other aponeuroses some differences could be observed. Ap2 is absent and Ap3 inserts on the the caudal ridge of the crista lateralis of the os palatinum, as Cr10 is absent in *P. oryzivora*.

Musculus pterygoideus ventralis medialis
Geospiza fortis (Fig. 9). The musculus pterygoideus ventralis medialis connects the caudal part of the os palatinum with the processus medialis mandibulae. It originates at the caudal part of the fossa ventralis of the os palatinum and at the processus pterygoideus palatini. It inserts with a tendon (T1) at the tip of processus medialis mandibulae.

Padda oryzivora (Fig. 10). Two aponeuroses could be distinguished. The first aponeurosis is similar to T1, but it is a vertical sheet that runs rostrally to insert on the proximal end of the processus pterygoideus palatini. A second aponeurosis (Ap2), which was not observed in *G. fortis*, attaches in the middle of the ventral side of the processus medialis mandibulae and runs rostrally.

Musculus pterygoideus dorsalis lateralis
Geospiza fortis (Fig. 9). The big musculus pterygoideus dorsalis lateralis runs from the os palatinum to the lower jaw and fills up the dorsolateral surface of the os palatinum completely. The muscle inserts on the lamella dorsalis of the os palatinum, is bordered by the crista dorsolateralis and extends to the pterygopalatine joint. More rostrally the muscle inserts on the dorsal, lateral and ventral side of the processus praemaxillaris palatini. Its fibers run lateroventrocaudally to insert between Cr19 and Cr20, ventral to the insertion of the musculus pseudotemporalis profundus. The muscle comprises four large aponeuroses, which will be numbered from ventral to dorsal. The first aponeurosis (Ap1) is a large aponeurosis that inserts on Cr20 on the medial side of the lower jaw and on the rostroventral edge of the processus medialis mandibulae. The aponeurosis covers the ventral side of the muscle and the dorsal, lateral and ventral side of the rostral-most part of the muscle that lies around the processus praemaxillaris palatini. To the caudal half of Cr10 of the processus transpalatinus of the os palatinum inserts a second aponeurosis (Ap2), which runs caudally. A third aponeurois (Ap3) attaches to the caudal ridge of the processus mandibulae medialis and runs rostrally. The last aponeurosis (Ap4) attaches to Cr19 running up to tuberculum pterygoidei and forms the dorsal border of the muscle.

Padda oryzivora (Fig. 10). Only two aponeuroses could be observed, the first one of which is similar to Ap2 but inserting on the caudal ridge of the processus transpalatinus. The second one is similar to Ap4 of *G. fortis*.

Musculus pterygoideus dorsalis medialis
Geospiza fortis (Fig. 9). The musculus pterygoideus dorsalis medialis covers the os pterygoideum, running from the pes pterygoidei to just rostral of the quadratomandibular joint. The muscle originates from all sides of the os pterygoideum, with more fibers attaching on the rostral side, and from the lateral and ventral side of the pes pterygoidei and attaches to the lower jaw. A first tendon (T-Ap1) inserts on the tuberculum pterygoidei on the medial side of the lower jaw and lies in line with the Ap4 of the musculus pterygoideus dorsalis lateralis. At its origin the tendon extends somewhat caudally forming a small aponeurosis. Muscle fibers run almost mediodorsally from T-Ap1 to insert on the os pterygoideum. The dorsal side of the muscle is formed by a second aponeurosis (Ap2), which also inserts on the tuberculum pterygoidei. Medially this muscle is bordered by a third aponeurosis (Ap3), which attaches on the caudomedial side of the pes pterygoidei and runs caudally. The medial surface of this aponeurosis receives muscle fibers of the musculus retractor palatini.

Padda oryzivora (Fig. 10). No differences could be observed.

Musculus retractor palatini
Geospiza fortis (Fig. 9). The musculus retractor palatini runs from the distinct Cr9 on the rostroventral side of the braincase to the caudal part of the pes pterygoidei. A vertically oriented aponeurosis (Ap1) originates on the dorsal side of the processus pterygoidei palatini and runs through the muscle with muscle fibers attaching on both sides. Its fibers also attach to the medial side of the large Ap3 of the musculus pterygoideus dorsalis medialis.

Padda oryzivora (Fig. 10). No differences could be observed.

Musculus protractor pterygoidei et quadrati
Geospiza fortis (Fig. 9). The small musculus protractor pterygoidei et quadrati originates on the lateral surface of the septum interorbitale, in fossa F1. It runs laterally to insert tendinously (T1) on the processus dorsalis of the os pterygoideum and the mediocaudal side of the os quadratum. T1 forms the rostral border of the muscle, with muscle fibers attaching to it and running almost mediodorsally to insert on the braincase in F1. Several fibers of the ventrocaudal side of the muscle run dorsally to attach to the os quadratum.

Padda oryzivora (Fig. 10). No differences could be observed.

Discussion

In this study, the head morphology of the Java finch (*P. oryzivora*) was compared with that of the medium ground finch (*G. fortis*). Although both species have a prokinetic skull with a rather similar morphology and a similar beak size, the skull of *G. fortis* is generally more robust with more prominent processes and cristae being present. The more robust head skeleton with firm processes and ridges

gives *G. fortis* better developed attachment sites for the bigger muscles. As both species have a similar muscle insertion and orientation, the higher bite force measured in *G. fortis* is suggested to be the direct result of the increase in muscle mass in *G. fortis*, being almost two–three times greater than in *P. oryzivora*. The increased robustness of the head skeleton and musculature of *G. fortis* is likely related to the hardness and size of seeds crushed by these species in the wild (De Leon et al. 2011). The hardest seeds eaten by *G. fortis* on Santa Cruz Island are of an average hardness of about 45 N, with a maximum hardness of some of the seeds that are cracked by these birds reaching up to 100 N (De Leon et al. 2011). Although data for the hardness of seeds consumed by *P. oryzivora* in the wild are not available, van der Meij & Bout (2000) estimated the maximal hardness of seeds that could still be cracked by *P. oryzivora* to be about 60 N. Thus, *G. fortis* appears to be able to crack harder seeds than *P. oryzivora*, and consequently needs to be able to produce a larger bite force. Note, however, that our *P. oryzivora* were captive-bred specimens, which may affect the development of muscle mass and corresponding bony structures due to a relaxed selection of bite force capacity in captivity. The measurements from Herrel et al. (2005a) show that *G. fortis* has a maximum bite force of 47 N. Our measurements of bite forces in *P. oryzivora* suggest a maximum bite force of 8.86 N, which corresponds well to previously published data for this species (9.6 N; see van der Meij & Bout, 2006). Interestingly, both the data for the Java finch and the medium ground finch suggest that these species can crack seeds with a hardness greater than their maximum bite force. Possible explanations for this at first sight rather paradoxical result are: first, birds continuously manipulate and reorientate the seed in their beak until they find the weakest spot to crack it (Ziswiler, 1965; van der Meij & Bout, 2000) in contrast to our measurements, which crack seeds in a single standardized orientation; second, the repeated biting results in micro-cracking ultimately resulting in failure of the seed. Interestingly, a comparison of the muscle masses with previously published data for a wide array of finches (van der Meij & Bout, 2004; Clabaut et al. 2009; see Fig. 11) illustrates the unique nature of the size of the jaw adductors and upper beak retractors in *G. fortis* being about three times the average mass typically observed in seed-cracking birds. This suggests that selection on seed-cracking capacity in the medium ground finch is unusually high. Another interesting observation is the great variability in jaw adductor muscle mass observed in *G. fortis* compared with *P. oryzivora*. This observation corresponds well to the previously described variability in head and beak size, and bite force in this species (Grant, 1986; Herrel et al. 2005a), and suggests a potential link between adductor mass, bite force capacity and beak size.

On an anatomical level, the most remarkable difference between the two species examined here is the absence of the ligamentum postorbitalis in *G. fortis* and consequently

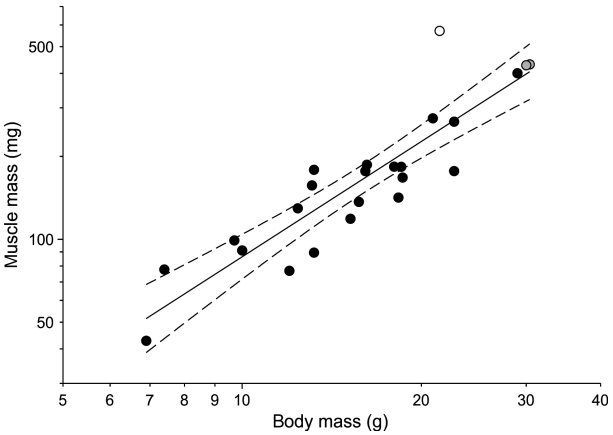

Fig. 11 Scatterplot illustrating the correlation between cranial muscle mass and body mass in seed-cracking birds. Gray symbols represent data for *Padda oryzivora*; the white symbol represents *Geospiza fortis*. Note how *G. fortis* has a significantly greater cranial muscle mass compared with other seed-cracking birds. Illustrated are the regression line and its 95% confidence limits. Note the log axes. Data taken from van der Meij & Bout (2004) and Clabaut et al. (2009).

the presence of a shorter processus postorbitalis. Although different previous workers (Bock, 1964; Bühler, 1981) suggested that this ligament has an important role in the cranial kinesis of birds as it is thought to couple the movements of the lower jaw to those of the upper jaw, Nuijens et al. (2000) demonstrated that a transsection of this ligament has only a slight effect on the husking performance in the zebra finch (*Taeniopygia guttata*). Bout & Zweers (2001) proposed the hypothesis that the absence of this ligament has only a limited influence on the degree and nature of kinesis present. In both *G. fortis* and *P. oryzivora* the form of cranial kinesis is prokinesis, in which the upper jaw pivots about the frontonasal hinge, without changing its shape. The movements of all the functional units, i.e. the os quadratum, the upper jaw, the palate, the os pterygoideum and the jugal bars, are coupled in such a way that a forward movement of the os quadratum exerts force through the jugal bar and os pterygoideum/palate to the upper jaw and thus causes the latter to swing dorsad. A backward movement of the os quadratum will result in an opposite movement of the same elements (Bock, 1964; Bühler, 1981; Zusi, 1993; Bout & Zweers, 2001; Gussekloo et al. 2001). We suggest that the absence of this ligament and a less developed processus postorbitalis in *G. fortis* might be linked to the need for additional space to accommodate the large musculus adductor mandibulae externus.

The two large tubercles of the processus coronoideus of the lower jaw of *G. fortis* differ from those in *P. oryzivora* where they are smaller and more caudally positioned. The third tubercle that is visible on the dorsal side of the lower jaw in *G. fortis* is the tuberculum pseudotemporalis. The position and shape of the tuberculum pseudotemporalis differs strongly between both species. In *G. fortis* this is a

well-developed tubercle onto which both parts of the musculus pseudotemporalis superficialis attach. In *P. oryzivora*, this tubercle is small and lies very close to the second tubercle of the processus coronoideus, and only the lateral part of the musculus pseudotemporalis superficialis attaches to it. Nuijens & Zweers (1997) labeled this tubercle as processus coronoideus in the spice finch (*Lonchura punctulata*), yet labeled it as the tuberculum pseudotemporalis in the greenfinch (*Carduelis chloris*). Probably, its position situated close to the processus coronoideus in the spice finch caused this confusion. Our dissections, however, demonstrate that the musculus pseudotemporalis superficialis lateralis does not attach to this tubercle in *P. oryzivora*, but to the tubercle lying medially of the second tubercle of the processus coronoideus, and that it is the musculus pterygoideus dorsalis medialis that attaches to this tubercle. Hence, we introduced a new name for the latter tubercle, i.e. tuberculum pterygoidei, which is also present in *G. fortis*, and can also be observed when inspecting the drawings of the greenfinch and spice finch in Nuijens & Zweers (1997) and the pictures of the other Darwin's finches of Bowman (1961). Another difference between *G. fortis* and *P. oryzivora* resides in the insertion of the musculus pseudotemporalis superficialis medialis on the lower jaw. In *P. oryzivora* this insertion is situated dorsal to the fenestra mandibulae caudalis [labeled by Nuijens & Zweers (1997) as the fenestra rostralis mandibulae], while in *G. fortis* this insertion is restricted to one point, the rostral side of the tuberculum pseudotemporalis. In that way, the line of action of the musculus pseudotemporalis superficialis medialis differs, running rostrolaterally in *P. oryzivora*, but nearly entirely laterally in *G. fortis*. This suggests a more medially directed force component of this muscle in *G. fortis,* which may assist in the manipulation and cracking of seeds, as seed cracking involves lateral movements of the lower jaw. However, the lack of functional data on the activation patterns of the jaw muscles and jaw movements during cracking prevent us from addressing this hypothesis in any detail.

The most striking difference between the palate and upper jaw of *G. fortis* and those of *P. oryzivora* is probably the absence of the processus palatinus praemaxillae in *P. oryzivora* and its wider nature of the processus praemaxillaris palatini. However, the wider processus praemaxillaris palatini of *P. oryzivora* [or of *L. punctulata* in Nuijens & Zweers (1997), where it is called the 'processus maxillaris'] probably results from a fusion of it with the processus palatinus maxillae. Such a fusion has been described by Jollie (1957) in the American robin (*Turdus migratorius*) and the English sparrow (*Passer domesticus*). The attachment of the most rostral tendon of the musculus pterygoideus ventralis lateralis to the rostrolateral edge of the processus praemaxillae palatini in *P. oryzivora* also suggests that this part is homologous with the processus palatinus maxillae. Not only does the processus praemaxillaris palatini differ between both species, also the processus transpalatinus is flatter and wider in *P. oryzivora*.

The ossa palatina of both bird species also differ in their articulation with the os pterygoideum. In *G. fortis*, an articulation facet between the os pterygoideum and the os palatinum is present, whereas the os pterygoideum and the os palatinum of *P. oryzivora* are partially fused, resulting in an articulation and a flexion zone between the os pterygoideum and the os palatinum. Following Zusi & Livezey (2006), this may be due to the presence of a 'pars palatina pterygoidei' (a rostrodorsal splint of the os pterygoideum above the dorsal edges of the os palatinum) that is ventrally fused with the os palatinum and rostral with the os vomer. Following the theory of Zusi & Livezey (2006), this would mean that the pes pterygoidei in *G. fortis* is separated from this pars palatina pterygoidei by an articulatio intrapterygoidea, but in *P. oryzivora* this separation is only partial, resulting in a flexion zone and an articulation between the two parts of the os pterygoideum. However, because of the fact that the fusion between the os palatinum and the os pterygoideum in *P. oryzivora* is only partial as well as narrow, it can be inferred that the reduction in kinesis in this species would be small (B. Livezey, pers. commun.). Also the contact between the processus maxillopalatinus and the os vomer is only found in *P. oryzivora*, but would also not influence the cranial kinesis, according to Bock (1964).

In summary, despite the overall similarity in beak size and cranial morphology, differences in the jaw adductor size and corresponding attachments to the cranium and mandible are prominent, with *G. fortis* having much more robust jaw-closing muscles. This is reflected in differences in bite forces, with *G. fortis* biting much harder than *P. oryzivora*. These data suggest similarities in the evolution of the feeding system in birds specializing on cracking hard seeds, as muscle orientation and organization and the overall cranial morphology are similar, but also show the uniqueness of the robustness of the cranial morphology and bite force of *G. fortis* compared with other seed-cracking birds. As such, *P. oryzivora* may not be an ideal functional analog for the Galápagos ground finches. Yet, the similarity in beak size and overall morphology suggests that it could provide useful insights into the mechanics of beak movement in seed-cracking birds in general. Future studies investigating the anatomy and development of the jaw system in a variety of seed-cracking birds would be extremely insightful in our understanding of the jaw system in ground finches of the genus *Geospiza*, and the structural adaptations related to seed cracking in birds more generally.

Acknowledgements

Fieldwork was coordinated through the Charles Darwin Research Station and the Galápagos National Park Service. The authors thank Eric Hilton, Sarah Huber and Bieke Vanhooydonck for their

assistance in the field and for helping collect road-killed specimens. This work was supported by NSF grant IBN-0347291 to J.P., by an interdisciplinary research grant of the special research fund of the University of Antwerp to P.A., J.D., A.G. and A.H., and by a PHC Tournesol collaborative grant to D.A. and A.H. The UGCT scanning facility acknowledges the support from the Ghent University special research fund (BOF).

Author contributions

CT-scanning: Matthieu Boone, Luc Van Hoorebeke; acquisition of material: Anthony Herrel, Jeffrey Podos; 3D-reconstruction: Annelies Genbrugge; dissections: Annelies Genbrugge, Anthony Herrel; drafting of the manuscript: Annelies Genbrugge, Anthony Herrel; help in methods: Dominique Adriaens, Peter Aerts, Anthony Herrel; critical revision of the manuscript: all authors.

References

Abzhanov A, Protas M, Grant BR, et al. (2004) Bmp4 and morphological variation of beaks in Darwin's finches. *Science* **305**, 1162–1464.

Abzhanov A, Kuo WP, Hartmann C, et al. (2006) The Calmodulin pathway and evolution of elongated beak morphology in Darwin's finches. *Nature* **442**, 563–567.

Azizi E, Brainerd EL, Roberts TJ (2008) Variable gearing in pennate muscles. *Proc Natl Acad Sci* **105**, 1745.

Baumel JJ, King AS, Lucas AM, et al. (1979) *Nomina Anatomica Avum*, pp. 53–219. London: Academic Press.

Boag PT, Grant PR (1981) Intense natural selection in a population of Darwin's finches (Geospizinae) in the Galápagos. *Science* **214**, 82–85.

Bock WJ (1963) Morphological differentiation and adaptation in the Galapagos finches. *Auk* **80**, 202–207.

Bock WJ (1964) Kinetics of the avian skull. *J Morphol* **114**, 1–42.

Bout RG, Zweers GA (2001) The role of cranial kinesis in birds. *Comp Biochem Physiol A* **131**, 197–205.

Bowman RI (1961) Morphological differentiation and adaptation in the Galapagos finches. *Univ Calif Publ Zool* **58**, 1–302.

Bühler P (1981) 8 Functional anatomy of the avian jaw apparatus. In: *Form and Function in Birds*, pp. 439–468. London: Academic Press.

Clabaut C, Herrel A, Sanger T, et al. (2009) Development of beak polymorphism in the African Seedcracker, *Pyrenestes ostrinus*. *Evol Dev* **11**, 636–646.

Colnett J (1798) *A Voyage to the South Atlantic and Round Cape Horn into the Pacific Ocean: for the Purpose of Extending the Spermaceti Whale Fisheries, and Other Objects of Commerce, by Ascertaining the Ports, Bays, Harbours, and Anchoring Births, in Certain Islands and Coasts in those Seas, at which the Ships of the British Merchants might be Refitted/Undertaken and Performed by Captain James Colnett, of the Royal Navy, in the ship Rattler*. London: W. Bennett.

Cutts A (1988) The range of sarcomere lengths in the muscles of the human lower limb. *J Anat* **160**, 79–88.

Darwin CR (1841) *The Zoology of the Voyage of H.M.S. Beagle, Under the Command of Captain FitzRoy R.N. During the Years 1832–1836. Part III: Birds*. London: Smith Elder.

De Leon LF, Raeymaekers JAM, Bermingham E, et al. (2011) Exploring possible human influences on the evolution of Darwin's finches. *Evolution* **65**, 2258–2272.

Foster DJ, Podos J, Hendry AP (2008) A geometric morphometric appraisal of beak shape in Darwin's finches. *J Evol Biol* **21**, 263–275.

Grant PR (1986) *Ecology and Evolution of Darwin's Finches*, p. 492. Princeton, New Jersey: Princeton University Press.

Grant PR, Grant BR (2002) Unpredictable evolution in a 30-year study of Darwin's finches. *Science* **296**, 707–711.

Grant PR, Grant BR (2008) *How and Why Species Multiply: the Radiation of Darwin's Finches*, p. 218. Princeton, New Jersey: Princeton University Press.

Gussekloo SWS, Vosselman MG, Bout RG (2001) Three-dimensional kinematics of skeletal elements in avian prokinetic and rhynchokinetic skulls determined by roentgen stereophotogrammetry. *J Exp Biol* **204**, 1735–1744.

Herrel A, Podos J, Huber SK, et al. (2005a) Bite performance and morphology in a population of Darwin's finches: implications for the evolution of beak shape. *Funct Ecol* **19**, 43–48.

Herrel A, Podos J, Huber SK, et al. (2005b) Evolution of bite force in Darwin's finches: a key role for head width. *J Evol Biol* **18**, 669–675.

Herrel A, Soons J, Aerts P, et al. (2010) Adaptation and function of Darwin's finch beaks: divergence by feeding type and sex. *Emu* **110**, 39–47.

Jollie MT (1957) The head skeleton of the chicken and remarks on the anatomy of this region in other birds. *J Morphol* **100**, 389–436.

Jønsson KA, Fjeldså J (2006) A phylogenetic supertree of oscine passerine birds (Aves: Passeri). *Zool Scr* **35**, 149–186.

Kleindorfer S, Chapman TW, Winkler H, et al. (2006) Adaptive divergence in contiguous populations of Darwin's small ground finch (*Geospiza fuliginosa*). *Evol Ecol Res* **8**, 357–372.

Litchwark GA, Bougoulias K, Wilson AM (2007) Muscle fascicle and series elastic element length changes along the length of the human gastrocnemius during walking and running. *J Biomech* **40**, 157–164.

Loeb GE, Gans C (1986) *Electromyography for Experimentalists*. Chicago: University of Chicago Press.

van der Meij MAA, Bout RG (2000) Seed selection in the Java sparrow (*Padda oryzivora*): preference and mechanical constraint. *Can J Zool* **78**, 1668–1673.

van der Meij MAA, Bout RG (2004) Scaling of jaw muscle size and maximal bite force in finches. *J Exp Biol* **207**, 2745–2753.

van der Meij MAA, Bout RG (2006) Seed husking time and maximal bite force in finches. *J Exp Biol* **209**, 3329–3335.

Méndez J, Keys A (1960) Density and composition of mammalian muscle. *Metabolism* **9**, 184–188.

Muhl ZF (1982) Active length-tension relation and the effect of muscle pinnation on fiber lengthening. *J Morphol* **173**, 285–292.

Nuijens FW, Zweers GA (1997) Characters discriminating two seed husking mechanisms in finches (Fringillidae: Carduelinae) and Estrildids (Passeridae: Estrildinae). *J Morphol* **232**, 1–33.

Nuijens FW, Hoek AC, Bout RG (2000) The role of the postorbital ligament in the zebra finch (*Taeniopygia guttata*). *Neth J Zool* **50**, 75–88.

Podos J, Nowicki S (2004) Beaks, adaptation and vocal evolution in Darwin's finches. *Bioscience* **54**, 501–510.

Schluter D (1982) Seed and patch selection by Galápagos ground finches: relation to foraging efficiency and food supply. *Ecology* **63**, 1106–1120.

Schluter D (1984) Morphological and phylogenetic relations among Darwin's finches. *Evolution* **38**, 921–930.

Schluter D (2000) The ecology of adaptive radiation. *Oxford Series in Ecology and Evolution*. Oxford: Oxford University Press.

Soons J, Herrel A, Genbrugge A, et al. (2010) Mechanical stress, fracture risk and beak evolution in Darwin's ground finches (Geospiza). *Philos Trans R Soc Lond B Biol Sci* **365**, 1093–1098.

Vlassenbroeck J, Dierick M, Masschaele B, et al. (2007) Software tools for quantification of X-ray microtomography at the UGCT. *Nucl Instrum Methods Phys Res A* **580**, 442–445.

Ziswiler V (1965) Zur Kenntnis des Samenöffnens und der Struktur des hörnernen Gaumens bei körnerfressenden Oscines. *J Ornithol* **106**, 1–48.

Zusi RL (1993) Patterns and diversity in the avian skull. In: *The Skull. Volume 2. Patterns of Structural and Systematic Diversity* (eds Hanken J, Hall BK), p. 566. Chicago: The University of Chicago Press.

Zusi RL, Livezey BC (2006) Variation in the os palatinum and its structural relation to the palatinum osseum of birds (Aves). *Ann Carnegie Mus* **75**, 137–180.